ACS APPLIED ENERGY MATERIALS

www.acsaem.org Article

Bimetallic Copper–Silver Catalysts for the Electrochemical Reduction of CO_2 to Ethanol

Elisabeth Robens,* Burkhard Hecker, Hans Kungl, Hermann Tempel, and Rüdiger-A. Eichel

Cite This: ACS Appl. Energy Mater. 2023, 6, 7571–7577 Read Online

ACCESS | Metrics & More | Article Recommendations

ABSTRACT: The electrochemical reduction of carbon dioxide to ethanol is a promising way to make CO_2 electrolysis economically feasible. In this work, a bimetallic catalyst of silver and copper is synthesized, and the effect of its copper content on the formation of ethanol is analyzed. By decreasing the near-surface copper content from 99 to 45% (measured by XPS) at a current density of −20 mA cm^{-2}, the Faradaic efficiency of ethanol could be enhanced from 5 to 23%. Moreover, we show that with excess of CO, due to a lower copper and a higher silver near-surface content, the formation of ethanol is favored over ethylene.

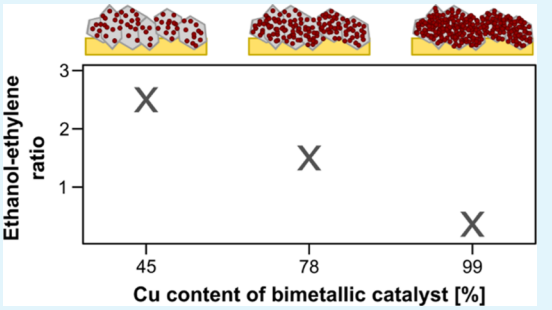

KEYWORDS: *CO_2 reduction, electrocatalysis, bimetallic catalyst, Cu, Ag, ethanol, electroless plating*

INTRODUCTION

The electrochemical reduction of carbon dioxide (CO_2) is a promising approach for harnessing the greenhouse gas CO_2 and thus producing climate-neutral carbon-based base chemicals.[1−3] The formed products in this process strongly depend on the used catalyst material. Copper has the great advantage of possessing an intermediate binding energy for the reaction intermediate *CO and thus can catalyze C−C coupling reactions.[4,5] This leads to the formation of value-added products with more than one carbon atom such as ethylene, ethanol, acetate, and *n*-propanol.[6−8]

The requirement for an economical CO_2 electrolysis process is a good compromise between a profitable niche market and an impactful mass market.[4] This is the case for ethanol. Therefore, the task is to tune copper catalysts to achieve higher Faradaic efficiencies (FEs) for ethanol.

Today, most copper-based catalysts favor the formation of ethylene over ethanol. For example, an ethanol-to-ethylene ratio in the range of about 0.3 to 0.5 for a modified copper surface is reported.[9] Also a ratio in the range of 0.25 to 1 for a Cu(I) oxide surface and a polycrystalline copper surface, respectively, is found.[6,10] The ranges reported represent results of different experimental parameters.

The reaction path on copper is extensively discussed in the literature and is influenced by many parameters. However, there is agreement that the key reaction intermediate of all products, except formate, is carbon monoxide.[6,11−14] Therefore, a promising approach exists in the usage of a bimetallic catalyst consisting of copper and a CO-forming material such as Ag, Au, or Zn. The CO-forming material should increase the amount of CO and therefore shift the selectivity of copper to more value-added C_2 products (see Scheme 1).[4,15,16]

Scheme 1. Simplified Reaction Pathway of CO_2RR to C_2 Products on a Bimetallic Cu/Ag Catalyst

$$CO_2 \xrightarrow{Ag,\ Cu} CO \xrightarrow{Cu} C_2$$

In this study, this approach is followed by using silver nanoplates (Ag NPls) as a basic structure that consists of a CO-selective silver catalyst with high activity due to its nanostructured surface.[17−19] Additionally, copper is deposited on the Ag NPls to obtain a shared copper−silver surface and thus enhancing the electrocatalytic kinetics. For the study of pure Ag NPls, we refer to another publication of ours.[19]

In the following, we report the synthesis of the new bimetallic catalyst, discuss its morphology, various compositions, and activities of the catalysts and analyze their catalytic performance in the CO_2 reduction under different conditions.

EXPERIMENTAL SECTION

Preparation of Bimetallic Cu−Ag Catalysts. All chemicals were used as obtained without any further purification. To synthesize

Received: April 19, 2023
Accepted: June 22, 2023
Published: July 11, 2023

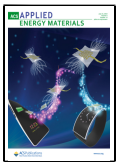

the bimetallic catalyst, Ag NPls were first fabricated as a basic structure in a two-step synthesis according to the work of Muench et al. and as we reported previously.[17−19] For this, silver seeds were formed by reducing silver ions with tin(II) chloride on the surface of silver foils (Scheme 2 "seeding"). Afterward, the anisotropic Ag NPl

Scheme 2. Two-Step Synthesis of Ag NPls and the Subsequent Copper Deposition[18−21]

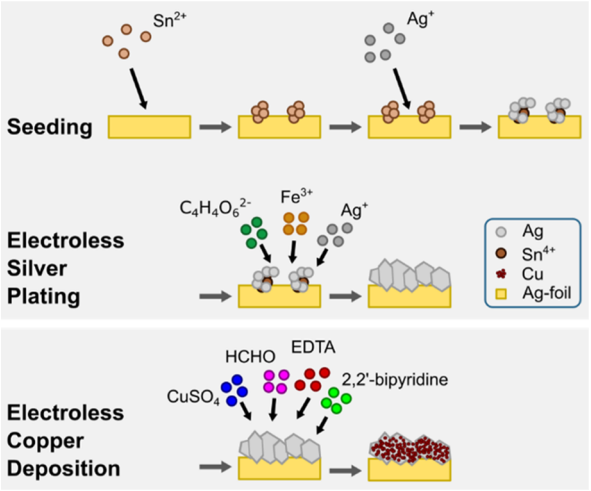

growth was supported by an Fe(III)−hydroxide−tartrate complex, which acts as a surface agent (Scheme 2 "electroless silver plating"). In our previously published paper, further details on this process can be found.[19] Subsequently, Ag NPls were partially covered by copper with the help of electroless copper deposition (Scheme 2 "electroless copper deposition"). For this, an aqueous copper bath consisting of formaldehyde (0.1 mol L^{-1}, 37%, BP, USP, Merck), copper sulfate pentahydrate (0.05 mol L^{-1}, ≥99%, VWR), ethylenediaminetetraacetic acid (0.1 mol L^{-1}, 99.4−100.6%, Sigma-Aldrich), and 2,2′-bipyridine (32 μmol L^{-1}, ACS, Merck) analogous to the work of Lee, Syu and Chen et al. was used.[20,21] The pH value of the solution was adjusted between 11.5 and 13.5 by adding sodium hydroxide platelets (≥98%, Sigma-Aldrich) and the bath was purged with nitrogen for 15 min. Afterward, the silver foil with the silver structure on top was inserted into the copper bath. In contact with the Ag NPls, the copper ions were reduced by formaldehyde in an alkaline solution. The Ag NPls acted as a catalyst for the reaction.[20,21] Therefore, the reduction of copper occurs only on the surface of the Ag NPls and not in solution. Thus, the separation of the solution after the reaction was simple since no elemental copper remained in the solution. The amount of copper on the surface of the Ag NPls was controlled by the duration of the electroless copper deposition. The duration was varied between 1 s and 15 min.

Catalyst Characterization. SEM images of the catalysts were acquired using a Quanta FEG 650 instrument from FEI (Hillsboro, Oregon, USA). The samples were scanned at a distance of 10 mm with an accelerating voltage of 20 kV, and the secondary electrons were sensed by an Everhart−Thornley detector. For the cross-sectional image of the catalyst, the sample was embedded in resin, cut transversely, and polished. To achieve better electrical conductivity, the resin-embedded catalyst was attached to the sample holder with copper tape.

The EDX measurements were performed using the same instrument as for SEM. For the analysis, an Octane Super detector from EDAX was applied using an acceleration voltage of 20 kV. The X-ray signals associated with the L-shells for copper and silver were used for analysis.

The D4 Endeavour instrument from Bruker (Indiana, USA) with a copper K-alpha source (1.5406 Å) was applied for XRD analysis. Measurements were performed at 40 kV and 40 mA in a Bragg−Brentano geometry between 10 and 130° with a step size of 0.01° and a counting time per step of 2 s.

To determine the total amount of copper in the catalyst, 0.5 cm^2 of the catalyst layer was first detached from the silver foil in an ultrasonic bath. The detached catalyst was then dissolved with concentrated HNO_3. The silver and copper contents were subsequently determined by ICP−MS (7900 ICP−MS, Agilent).

XPS measurements of the synthesized catalyst were carried out to analyze the near-surface composition. A Phi5000 VersaProbe II instrument (ULVAC-Phi Inc., USA) with a monochromatic Al K-alpha source (1.486 keV) was utilized for the XPS measurements. The analysis was performed in 0.8 eV steps, with each step lasting for 100 ms. The Shirley background was used for the analysis.

To investigate the altering of the catalyst, samples of the electrolyte were taken after 100 min of each CO_2 reduction reaction (CO_2RR) experiment. The copper content in the electrolyte was then analyzed by ICP−MS (7900, ICP−MS, Agilent).

Electrochemical CO_2RR. For the CO_2RR, a custom-made H-cell (Figure 1) separated by a Nafion 117 membrane and containing a

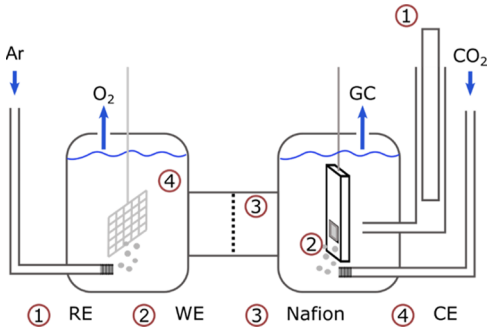

Figure 1. Sketch of the used H-cell for the electrochemical reduction of CO_2: RE, WE, CE, and GC. Note: For simplicity, the RE is drawn on the backside of the cathode; in reality, the RE points to the front side of the WE.

$KHCO_3$ electrolyte (0.1 mol L^{-1}, ≥99.7%, Honeywell) was used. Additionally, a platinum mesh and a commercial Ag/AgCl electrode (saturated) were applied as the counter electrode (CE) and reference electrode (RE), respectively.

The CO_2 gas inlet containing a frit with a pore size of 100 to 160 μm was positioned such that the gas bubbles entered the system on the front side of the working electrode (WE). The cathode compartment was filled with 55 mL and the anode compartment with 60 mL of electrolyte. Prior to the electrochemical measurements, the cathode and anode compartments were purged with carbon dioxide and argon, respectively, at a flow rate of 10 mL_n min^{-1} for 30 min. Argon is used to purge oxygen formed at the anode from the anolyte to prevent diffusion of small amounts of oxygen through the membrane to the cathode and subsequent reduction to oxygen. The cathode was inserted into the system with a custom-made Teflon sample holder that set the geometric surface area of the catalyst to 0.5 cm^2. To prevent the oxidation of the catalyst, a reductive potential of −0.9 V vs RE was already applied when the catalyst was inserted. For the electrochemical measurements, a VSP-300 potentiostat from Biologic was used. To determine the voltage (IR) drop between the RE and WE, a potentiostatic electrochemical impedance spectroscopy (PEIS) measurement was conducted, and the IR-corrected potential versus a reversible hydrogen electrode (RHE) was calculated according to eq 1

$$E_{\text{IR-corr.}}(\text{vs RHE}) = E(\text{vs Ag/AgCl}) + 0.197\ \text{V} + 0.0591\ \text{V}\cdot\text{pH-}IR \quad (1)$$

The pH of the electrolyte saturated with CO_2 was 6.8. After the PEIS measurement, a cyclic voltammetry (CV) measurement with a scanning rate of 20 mV s^{-1} was performed in the potential range of

https://doi.org/10.1021/acsaem.3c00985
ACS Appl. Energy Mater. 2023, 6, 7571−7577

−0.1 to −0.5 V vs RHE. The following CO_2RR was performed by chronopotentiometry at −20 mA cm^{-2} for 100 min or at varying current densities for 55 min.

The gaseous products of the CO_2RR were analyzed by gas chromatography (GC, Trace 1310, Thermo Scientific) every 15 min during the experiment. Additionally, liquid samples were taken after 55 and 100 min and were examined offline either by ion exclusion chromatography (IEC, S155, Sykam) for formate or by headspace gas chromatography (HS-GC, Trace 1310 with TriPlus 300 Headspace Autosampler) for the other liquid products. The IEC and HS-GC results were verified by ^1H NMR measurements with a water signal-suppressing method (Avance 600 MHz, Bruker).[6] The resulting FE for species i was calculated as follows

$$FE_i = \frac{n_i e_i F}{Q} \quad (2)$$

Here, n_i is the amount of product i, e_i is the number of electrons needed to produce one molecule of i, F is the Faradaic constant, and Q is the total amount of consumed charge.

RESULTS AND DISCUSSION

Catalyst Morphology, Composition, and Activity. The new bimetallic catalyst was synthesized by growing Ag NPls on silver foils followed by electroless deposition of copper (see the section "Preparation of Bimetallic Cu−Ag Catalysts"). The morphology was analyzed by taking SEM images of the top surface of the catalyst and the cross section (Figure 2a−c). The

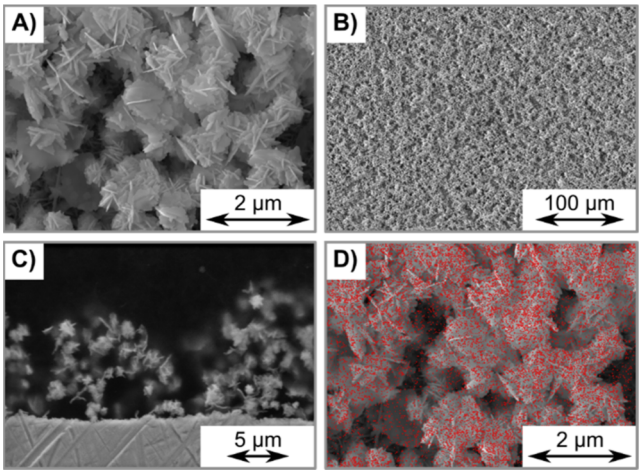

Figure 2. SEM images of the top surface of Cu/Ag nanoplates with 45% near-surface copper content (A,B) and a cross section of the resin-embedded catalyst with 90% near-surface copper content (C). Additionally, SEM/EDX overlay of Cu/Ag nanoplates with 45% near-surface copper content [(D), copper depicted in red].

images show that the catalyst consists of a porous catalyst film on the silver foil composed of silver plates with a nanoscale thickness forming a bead-like structure of 1 to 2 μm. The height of the catalyst layer can be determined to be 10 to 15 μm, and the beads form branched chains. For further information about the structure and properties of the Ag NPls, our previous publication is recommended.[19] The location of copper formed by electroless copper deposition can be visualized by overlaying the SEM image (Figure 2A) with copper EDX mapping. It can be seen that copper depicted in red was deposited on the Ag NPls (Figure 2D).

To determine the crystalline phase of the new bimetallic catalyst, the XRD pattern was measured (red line in Figure 3). For comparison, also an XRD measurement for pure Ag NPls

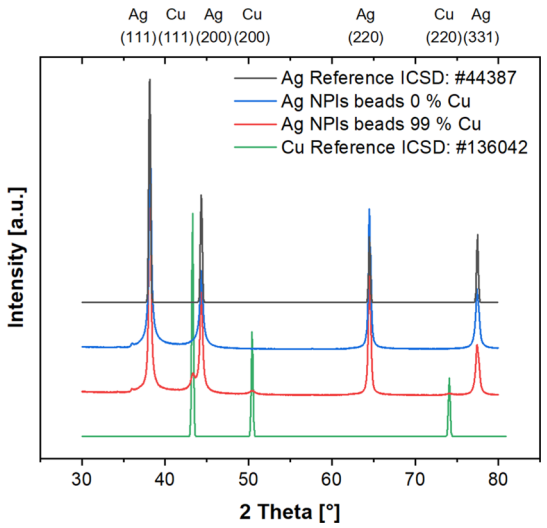

Figure 3. XRD patterns of Ag NPls and with copper-deposited Ag NPls. Additionally, XRD patterns from the ICS database[22] of silver and copper are shown. The copper content is determined by XPS.

(blue line) was performed, and reference data from the ICS database[22] for silver (black line) and copper (green line) are shown. The detected peaks indicate that the Ag NPls and the deposited copper have a polycrystalline structure. Moreover, the data show no shift in the silver peaks between the pure Ag NPl pattern (blue line) and that with copper (red line). Thus, with copper deposition, no changes in the lattice parameters of silver are observed.

To assess the synthesis and the respective electrocatalytic CO_2RR performance, systematic information about the near-surface copper content as a function of the total copper content has to be obtained. The copper content in the entire catalyst layer was measured by detaching the catalyst layer from the silver foil as described in the section "Catalyst Characterization" and subsequently analyzing the copper content by ICP−MS. Since this is a destructive method, additional non-destructive EDX measurements were performed prior to the electrochemical experiments and the final ICP−MS analysis. Plotting the two different copper contents against each other, a linear correlation is obtained, namely, $y = 1.81x$ (Figure 4A). This relation can be used as a calibration for a non-destructive determination of the total copper content using the EDX data. The near-surface copper content was obtained by XPS measurements (see the section "Catalyst Characterization"). The measured data are plotted versus the total copper content calibrated from the EDX data (Figure 4B). The near-surface copper content is higher than the average total copper content. This is reasonable since copper is only present on the surface of the catalyst due to the subsequent copper deposition on the Ag NPls. Moreover, the data show that bimetallic catalysts have been synthesized with a near-surface copper content ranging from 21 to 99%. Since the surface of the catalyst is the key area of the catalytic reaction, the near-surface copper content is used in the following to distinguish between the different catalyst samples.

To investigate whether the copper content was maintained during the reaction, the electrolyte after each CO_2RR experiment was analyzed for its copper content (see the section "Catalyst characterization"). Irrespective of the copper content of the tested catalyst, the averaged amount of dissolved copper was approximately 0.3 μg. Comparing this to the

https://doi.org/10.1021/acsaem.3c00985
ACS Appl. Energy Mater. 2023, 6, 7571−7577

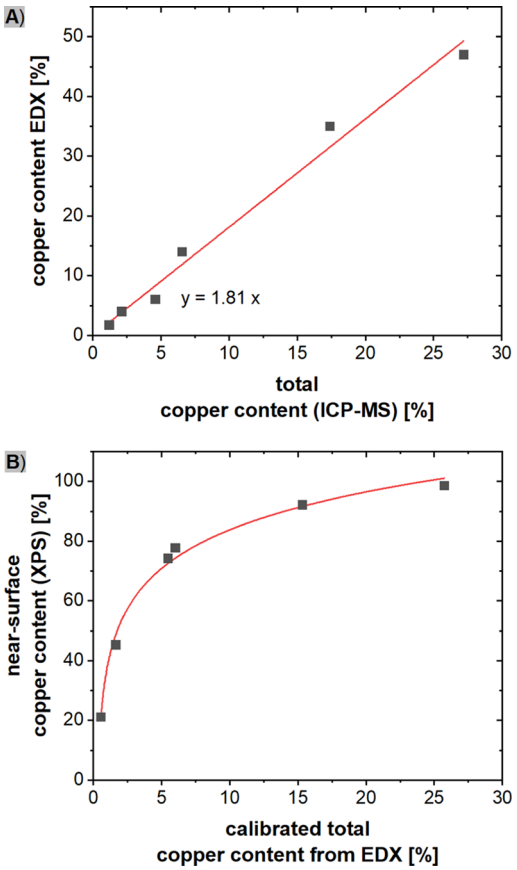

Figure 4. (A) Linear correlation between the copper content measured by EDX and the total copper content measured by ICP–MS. The red line represents the linear fit of the data. (B) Comparison of the total copper content (calibrated from EDX) and the near-surface (measured by XPS) copper content of several samples of the new bimetallic catalyst. The red line provides a guide-to-the eye for the reader.

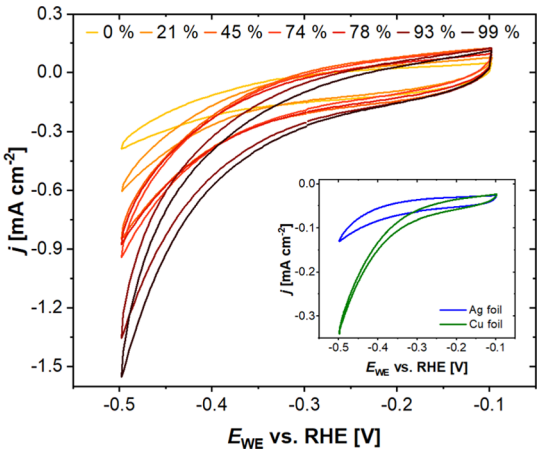

Figure 5. CV curves of the new bimetallic catalyst with different near-surface copper contents (see legend, measured by XPS). The measurements were performed in a potential range from −0.1 to −0.5 V vs RHE with a scan rate of 20 mV s^{-1} and in a 0.1 M $KHCO_3$ electrolyte. To ensure reproducibility, the given data are averaged values of at least two samples with similar near-surface copper content. The inset shows the CV curves for equally polished silver and copper foils as the reference.

catalyst with the lowest copper content, 7% of the copper is dissolved in the electrolyte during the reaction. In contrast, only 0.1% of copper is dissolved for the catalysts with the highest copper content.

The activity of a catalyst is a key factor for its performance.[23−27] Thus, the activity of the bimetallic catalysts with different copper contents was investigated by measuring the CV curves in the potential range from −0.1 to −0.5 V vs RHE with a scan rate of 20 mV s^{-1} and in a 0.1 M $KHCO_3$ electrolyte (Figure 5). The upper potential limit for these experiments was chosen to prevent oxidation of copper as this could alter the catalyst. To ensure reproducibility, the given data are averaged values of at least two samples with similar copper content. From −0.1 to −0.25 V vs RHE, the curves of the different samples are quite similar since in this potential range, mainly capacitive current and barely CO_2RR or hydrogen evolution reaction (HER) occurs. At more negative potentials, the reductive current density increases due to the starting CO_2RR and HER. With higher copper content, this effect is more pronounced. Possible reasons for higher current densities are a larger electrochemical surface area (ECSA) or a higher activity of the material. Tentatively, the ECSA should be identical for all catalyst specimens since the basic structure, namely, the Ag NPls, is the same for all catalysts. This is supported by similar double layer capacities (4.4 ± 0.8 mF cm^{-2}) for the different samples. Therefore, the reason for the increased reductive current density with higher copper content has to be an increased activity of the catalysts with a larger copper content. To support this hypothesis, CV curves were obtained with a silver and a copper foil polished under the same conditions (P4000 ultra-fine polishing paper) and therefore with an approximately identical ECSA (inset graph in Figure 5). The curves show a significantly higher reductive current density for the copper than for the silver foil, which is consistent with the above hypothesis.

Catalytic Performance in the CO_2RR. After the characterization of the new catalyst, its catalytic performance in the CO_2RR was tested. For this purpose, the catalysts with different near-surface copper contents ranging from 21 to 99% were measured at −20 mA cm^{-2} for 100 min (see the section "Electrochemical CO2 Reduction Reaction"). For simplicity, the near-surface copper content measured by XPS will be referred to only as copper content in the following. The gaseous and liquid samples taken over 100 min show relatively constant values. Therefore, a steady reaction over time can be assumed. The shown data are average values of at least two individual measurements. The error bars are calculated standard deviations considering the individual runs. Moreover, the respective potential at the working electrode, $E_{WE,IR\text{-}corr}$, was calculated using eq 1 and is indicated on the *x*-axis of Figure 6. The decrease in the magnitude of the potential with increasing copper content at constant current densities can be explained by the higher activity of the catalyst with higher copper contents (see the section "Catalyst morphology, composition, and activity"). The influence of the potential on the performance of the catalyst is analyzed at the end of this section.

Figure 6 shows that starting from the highest copper content of 99%, minimizing the copper content down to 45% results in a better-performing catalyst with less competitive and parasitic reduction of water to hydrogen (i.e., HER).[28,29] More specifically, the FE of hydrogen is decreased from 62 to 27%. Lowering the copper content even further does not show any additional improvements. The minimized hydrogen

https://doi.org/10.1021/acsaem.3c00985
ACS Appl. Energy Mater. 2023, 6, 7571−7577

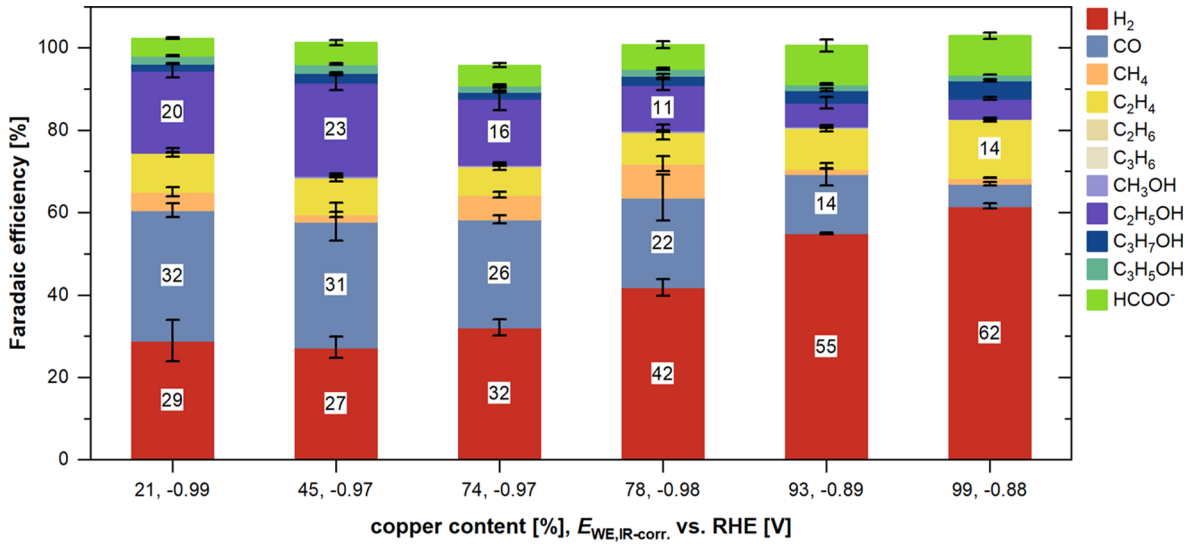

Figure 6. FE as a function of the near-surface copper content (measured by XPS). The experiments were performed at −20 mA cm^{-2} and for 100 min. The data are averaged over two to three individual measurements.

evolution can be explained by the following two facts. The amount of silver increases with decreasing copper content. This also enhances the formation of CO since silver surfaces mostly produce CO under these conditions.[30] As a result, the CO coverage of the copper surface is higher, leading to CO poisoning of the copper surface for the HER and thus to an enlarged CO_2RR.[4,31] Second, silver has a higher binding energy for the intermediate *H for the HER than copper.[5,32] Thus, the binding of *H on silver is less favored than on copper, and with it, the formation of hydrogen. A minimized copper content, therefore, lowers the HER. Furthermore, the data indicate that the ethanol formation, in contrast to the hydrogen evolution, is increased to 23% by decreasing the copper content down to 45%. Additionally, the ethanol-to-ethylene ratio is shifted from ethylene at higher copper contents to ethanol at lower copper contents.

If the ethanol-to-ethylene ratio is plotted versus the FE of CO, a systematic relation between the two quantities is observed (see Figure 7), clearly indicating an optimum for ethanol formation over the competitive ethylene formation. At levels of formed CO above 20%, the formation of ethanol starts being favored over the formation of ethylene. However, at amounts of CO larger than 30% and with decreasing copper content (below copper content = 21%), the favoring of ethanol is not further increased. Expressed in numbers, the ethanol-to-ethylene ratio is increased from 0.4 at an FE(CO) of 5.4% (copper content = 99%) to 2.6 at an FE(CO) of 30.5% (copper content = 45%). This observation nicely supports the suggested mechanism of Ting et al.: In excess of *CO, due to the high silver content, it is possible to selectively reduce CO to ethanol on Cu(111) surface orientations by an alternative reaction pathway. Here, instead of CO dimerization,[13] *CO reacts as a C−C coupling step with *CH_x (x = 1, 2) to *CH_xCO, which reacts selectively via the aldehyde *CH_3CHO to ethanol.[33] In summary, a copper-to-silver ratio of about 50:50 shows the most beneficial interplay of copper and silver with a decreased formation of hydrogen and an increased formation of ethanol.

To figure out if the catalyst performance could be further enhanced and to analyze the influence of the current density and the respective potential on the performance, the best-performing catalyst (45% copper) was tested at two additional current densities and corresponding potentials, namely, −10 mA cm^{-2} (−0.88 V vs RHE) and −30 mA cm^{-2} (−1.09 V vs RHE) (Figure 8). These measurements were conducted for 55 min, and the shown data are averages of three individual runs. At −10 mA cm^{-2}, the amount of CO is dramatically increased, while the formation of ethylene and ethanol is significantly decreased. For copper catalysts, the formation of C_2 products would already be expected at this potential,[6,34,35] as can also be observed for our catalyst with 99% Cu content (see Figure 7). However, comparing the data with bimetallic Cu/Ag catalysts, this behavior is in line with the literature.[33,36] In contrast, a more negative current density and potential (−30 mA cm^{-2}, −1.09 V vs RHE) results in higher hydrogen and methane evolution but lower CO formation. Simultaneously, the percentage of ethanol decreases slightly. The higher hydrogen formation can be explained by limited mass transport of CO_2

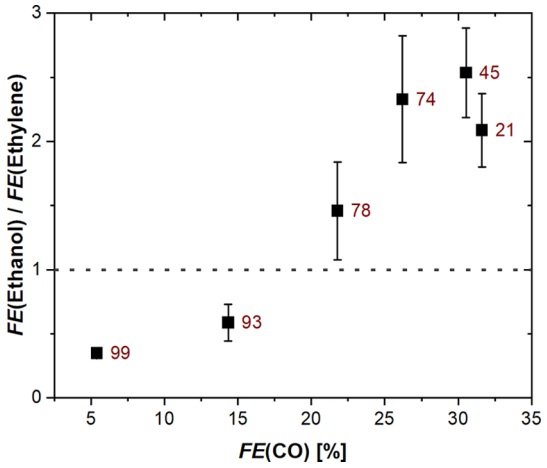

Figure 7. Correlation between the FE of CO and the ethanol-to-ethylene ratio. The red numbers represent the copper content (measured by XPS) of the used catalyst. The error bars are calculated by Gaussian error propagation from the errors of the FE of ethanol and ethylene. The dashed horizontal line marks the transition between the catalysts favoring ethylene (below) or ethanol (above) formation.

https://doi.org/10.1021/acsaem.3c00985
ACS Appl. Energy Mater. 2023, 6, 7571−7577

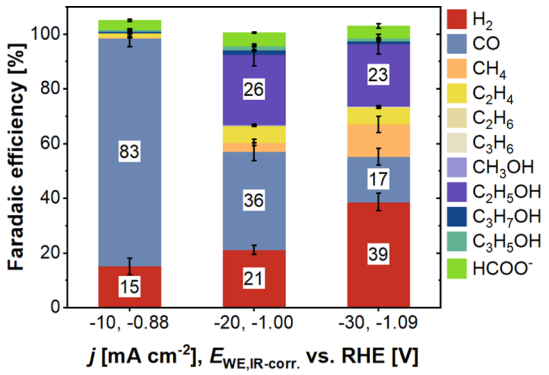

Figure 8. FE of 45% copper catalysts (measured by XPS) as a function of current density and potential at the working electrode. The measurements were performed for 55 min, and the data are averaged over three individual runs.

to the cathode at an increased negative current density. Moreover, the enhanced formation of methane is caused by the more negative potential, which is shown by the data of Kuhl et al., for instance.[6] This trend is consistent with the work of Ting and co-workers.[33] Since the amount of hydrogen should be minimal and that of ethanol maximal, −20 mA cm^{-2} and about −1.0 V vs RHE appear to be a suitable current density and potential, respectively, for CO_2 reduction with the used bimetallic catalyst and cell setup.

CONCLUSIONS

It was possible to perform a controlled synthesis of a new designed bimetallic catalyst consisting of Ag NPls partially coated with copper. By varying the duration of the electroless copper deposition, catalysts with different copper contents could be prepared. The catalysts were characterized by SEM, EDX, XPS, ICP−MS, and XRD. A linear relation was found between the copper content measured by EDX and by ICP−MS. With this relation, the copper content in the entire catalyst layer could be measured non-destructively. In addition, the activity of the catalyst was observed to rise with increasing near-surface copper content.

The influence of the copper content on the performance of the catalyst in the CO_2RR was investigated. When the near-surface copper content was gradually decreased from 99 to 45%, the amount of ethanol was enhanced from 5 to 23%, and the competing HER was minimized from 62 to 27%. Lowering the copper content even further does not show any additional improvements. However, not only the formation of ethanol could be increased by lowering the copper content down to 45% but also the selective formation of ethanol instead of ethylene. The ethanol/ethylene ratio could be increased from 0.4 to 2.6. A comparison of three different current densities showed that −20 mA cm^{-2} and about −1.0 V vs RHE are suitable conditions for the used catalyst and cell design.

AUTHOR INFORMATION

Corresponding Author

Elisabeth Robens − *Institute of Energy and Climate Research—Fundamental Electrochemistry (IEK-9), Forschungszentrum Jülich GmbH, 52425 Jülich, Germany; Institute of Physical Chemistry, RWTH Aachen University, 52056 Aachen, Germany;* orcid.org/0000-0003-3440-484X; Email: e.robens@fz-juelich.de

Authors

Burkhard Hecker − *Institute of Energy and Climate Research—Fundamental Electrochemistry (IEK-9), Forschungszentrum Jülich GmbH, 52425 Jülich, Germany;* orcid.org/0000-0003-0462-901X

Hans Kungl − *Institute of Energy and Climate Research—Fundamental Electrochemistry (IEK-9), Forschungszentrum Jülich GmbH, 52425 Jülich, Germany*

Hermann Tempel − *Institute of Energy and Climate Research—Fundamental Electrochemistry (IEK-9), Forschungszentrum Jülich GmbH, 52425 Jülich, Germany;* orcid.org/0000-0002-9794-6403

Rüdiger-A. Eichel − *Institute of Energy and Climate Research—Fundamental Electrochemistry (IEK-9), Forschungszentrum Jülich GmbH, 52425 Jülich, Germany; Institute of Physical Chemistry, RWTH Aachen University, 52056 Aachen, Germany;* orcid.org/0000-0002-0013-6325

Complete contact information is available at: https://pubs.acs.org/10.1021/acsaem.3c00985

Author Contributions

The manuscript was written through contributions of all authors. All authors have given approval to the final version of the manuscript.

Notes

The authors declare no competing financial interest.

ACKNOWLEDGMENTS

This work received funding by the German Federal Ministry of Education and Research (Bundesministerium für Bildung und Forschung, BMBF) under grant no. 03SF0627A "iNEW2.0 - Inkubator Nachhaltige Elektrochemische Wertschöpfungsketten". The authors thank SBC Lehmann for graphical support.

REFERENCES

(1) Rosen, J.; Hutchings, G. S.; Lu, Q.; Rivera, S.; Zhou, Y.; Vlachos, D. G.; Jiao, F. Mechanistic Insights into the Electrochemical Reduction of CO2 to CO on Nanostructured Ag Surfaces. *ACS Catal.* **2015**, *5*, 4293−4299.

(2) Jordaan, S. M.; Wang, C. Electrocatalytic Conversion of Carbon Dioxide for the Paris Goals. *Nat. Catal.* **2021**, *4*, 915−920.

(3) Jhong, H. R. M.; Ma, S.; Kenis, P. J. Electrochemical Conversion of CO2 to Useful Chemicals: Current Status, Remaining Challenges, and Future Opportunities. *Curr. Opin. Chem. Eng.* **2013**, *2*, 191−199.

(4) Nitopi, S.; Bertheussen, E.; Scott, S. B.; Liu, X.; Engstfeld, A. K.; Horch, S.; Seger, B.; Stephens, I. E. L.; Chan, K.; Hahn, C.; Nørskov, J. K.; Jaramillo, T. F.; Chorkendorff, I. Progress and Perspectives of Electrochemical CO2 Reduction on Copper in Aqueous Electrolyte. *Chem. Rev.* **2019**, *119*, 7610−7672.

(5) Bagger, A.; Ju, W.; Varela, A. S.; Strasser, P.; Rossmeisl, J. Electrochemical CO2 Reduction: A Classification Problem. *ChemPhysChem* **2017**, *18*, 3266−3273.

(6) Kuhl, K. P.; Cave, E. R.; Abram, D. N.; Jaramillo, T. F. New Insights into the Electrochemical Reduction of Carbon Dioxide on Metallic Copper Surfaces. *Energy Environ. Sci.* **2012**, *5*, 7050−7059.

(7) Hori, Y.; Takahashi, I.; Koga, O.; Hoshi, N. Selective Formation of C2 Compounds from Electrochemical Reduction of CO2 at a Series of Copper Single Crystal Electrodes. *J. Phys. Chem. B* **2002**, *106*, 15−17.

(8) Hori, Y.; Takahashi, I.; Koga, O.; Hoshi, N. Electrochemical Reduction of Carbon Dioxide at Various Series of Copper Single Crystal Electrodes. *J. Mol. Catal. A: Chem.* **2003**, *199*, 39−47.

(9) Zou, C.; Xi, C.; Wu, D.; Mao, J.; Liu, M.; Liu, H.; Dong, C.; Du, X. W. Porous Copper Microspheres for Selective Production of

Multicarbon Fuels via CO2 Electroreduction. *Small* **2019**, *15*, 1902582.
(10) Ren, D.; Deng, Y.; Handoko, A. D.; Chen, C. S.; Malkhandi, S.; Yeo, B. S. Selective Electrochemical Reduction of Carbon Dioxide to Ethylene and Ethanol on Copper(I) Oxide Catalysts. *ACS Catal.* **2015**, *5*, 2814−2821.
(11) Hori, Y.; Takahashi, R.; Yoshinami, Y.; Murata, A. Electrochemical Reduction of CO at a Copper Electrode. *J. Phys. Chem. B* **1997**, *101*, 7075−7081.
(12) Peterson, A. A.; Abild-Pedersen, F.; Studt, F.; Rossmeisl, J.; Nørskov, J. K. How Copper Catalyzes the Electroreduction of Carbon Dioxide into Hydrocarbon Fuels. *Energy Environ. Sci.* **2010**, *3*, 1311−1315.
(13) Kortlever, R.; Shen, J.; Schouten, K. J. P.; Calle-Vallejo, F.; Koper, M. T. M. Catalysts and Reaction Pathways for the Electrochemical Reduction of Carbon Dioxide. *J. Phys. Chem. Lett.* **2015**, *6*, 4073−4082.
(14) Garza, A. J.; Bell, A. T.; Head-Gordon, M. Mechanism of CO2 Reduction at Copper Surfaces: Pathways to C2 Products. *ACS Catal.* **2018**, *8*, 1490−1499.
(15) Lum, Y.; Ager, J. W. Sequential catalysis controls selectivity in electrochemical CO_2 reduction on Cu. *Energy Environ. Sci.* **2018**, *11*, 2935−2944.
(16) Romero Cuellar, N. S.; Scherer, C.; Kaçkar, B.; Eisenreich, W.; Huber, C.; Wiesner-Fleischer, K.; Fleischer, M.; Hinrichsen, O. Two-Step Electrochemical Reduction of CO2 towards Multi-Carbon Products at High Current Densities. *J. CO2 Util.* **2020**, *36*, 263−275.
(17) Muench, F.; Vaskevich, A.; Popovitz-Biro, R.; Bendikov, T.; Feldman, Y.; Rubinstein, I. Expanding the Boundaries of Metal Deposition: High Aspect Ratio Silver Nanoplatelets Created by Merging Nanobelts. *Electrochim. Acta* **2018**, *264*, 233−243.
(18) Muench, F.; Popovitz-Biro, R.; Bendikov, T.; Feldman, Y.; Hecker, B.; Oezaslan, M.; Rubinstein, I.; Vaskevich, A. Nucleation-Controlled Solution Deposition of Silver Nanoplate Architectures for Facile Derivatization and Catalytic Applications. *Adv. Mater.* **2018**, *30*, 1805179.
(19) Hecker, B.; Robens, E.; Valencia, H. E.; Windmüller, A.; Muench, F.. Tuning the Selectivity for the CO 2 Reduction towards CO through the Specific Synthesis of Silver Catalysts with Different Morphologies; *1*−*27*.
(20) Lee, C. L.; Syu, C. C. Ag Nanoparticle as a New Activator for Catalyzing Electroless Copper Bath with 2,2′-Bipyridyl. *Electrochim. Acta* **2011**, *56*, 8880−8883.
(21) Chen, C.-H.; Yang, H.-L.; Chen, H.-R.; Lee, C.-L. Activity on Electrochemical Surface Area: Silver Nanoplates as New Catalysts for Electroless Copper Deposition. *J. Electrochem. Soc.* **2012**, *159*, D507−D511.
(22) Zagorac, D.; Muller, H.; Ruehl, S.; Zagorac, J.; Rehme, S. Recent Developments in the Inorganic Crystal Structure Database: Theoretical Crystal Structure Data and Related Features. *J. Appl. Crystallogr.* **2019**, *52*, 918−925.
(23) Ma, W.; He, X.; Wang, W.; Xie, S.; Zhang, Q.; Wang, Y. Electrocatalytic Reduction of CO 2 and CO to Multi-Carbon Compounds over Cu-Based Catalysts. *Chem. Soc. Rev.* **2021**, *50*, 12897−12914.
(24) Endrődi, B.; Samu, A.; Kecsenovity, E.; Halmágyi, T.; Sebők, D.; Janáky, C. Operando Cathode Activation with Alkali Metal Cations for High Current Density Operation of Water-Fed Zero-Gap Carbon Dioxide Electrolysers. *Nat. Energy* **2021**, *6*, 439−448.
(25) Liu, S.; Tao, H.; Zeng, L.; Liu, Q.; Xu, Z.; Liu, Q.; Luo, J. L. Shape-Dependent Electrocatalytic Reduction of CO2 to CO on Triangular Silver Nanoplates. *J. Am. Chem. Soc.* **2017**, *139*, 2160−2163.
(26) Kim, C.; Jeon, H. S.; Eom, T.; Jee, M. S.; Kim, H.; Friend, C. M.; Min, B. K.; Hwang, Y. J. Achieving Selective and Efficient Electrocatalytic Activity for CO2 Reduction Using Immobilized Silver Nanoparticles. *J. Am. Chem. Soc.* **2015**, *137*, 13844−13850.
(27) Peng, X.; Karakalos, S. G.; Mustain, W. E. Preferentially Oriented Ag Nanocrystals with Extremely High Activity and Faradaic Efficiency for CO2 Electrochemical Reduction to CO. *ACS Appl. Mater. Interfaces* **2018**, *10*, 1734−1742.
(28) Jaster, T.; Gawel, A.; Siegmund, D.; Holzmann, J.; Lohmann, H.; Klemm, E.; Apfel, U. P. Electrochemical CO2 Reduction toward Multicarbon Alcohols - The Microscopic World of Catalysts & Process Conditions. *iScience* **2022**, *25*, 104010.
(29) Martić, N.; Reller, C.; Macauley, C.; Lo, M.; Reichert, A. M.; Reichbauer, T.; Vetter, K.; Schmid, B.; Mclaughlin, D.; Leidinger, P.; Reinisch, D.; Vogl, C.; Mayrhofer, K. J. J. Ag2Cu2O3 − a Catalyst Template Material for Selective Electroreduction of CO to C2+ Products. *Energy Environ. Sci.* **2020**, *13*, 2993.
(30) Hori, Y.; Wakebe, H. H. I.; Tsukamoto, T.; Koga, O. Electrocatalytic Process of CO Selectivity in Electrochemical Reduction of Co2 at Metal Electrodes in Aqueous Media. *Electrochim. Acta* **1994**, *39*, 1833−1839.
(31) Ooka, H.; Figueiredo, M. C.; Koper, M. T. M. Competition between Hydrogen Evolution and Carbon Dioxide Reduction on Copper Electrodes in Mildly Acidic Media. *Langmuir* **2017**, *33*, 9307−9313.
(32) Santos, E.; Pötting, K.; Lundin, A.; Quaino, P.; Schmickler, W. Hydrogen Evolution on Single-Crystal Copper and Silver: A Theoretical Study. *ChemPhysChem* **2010**, *11*, 1491−1495.
(33) Ting, L. R. L.; Piqué, O.; Lim, S. Y.; Tanhaei, M.; Calle-Vallejo, F.; Yeo, B. S. Enhancing CO2 Electroreduction to Ethanol on Copper-Silver Composites by Opening an Alternative Catalytic Pathway. *ACS Catal.* **2020**, *10*, 4059−4069.
(34) Handoko, A. D.; Ong, C. W.; Huang, Y.; Lee, Z. G.; Lin, L.; Panetti, G. B.; Yeo, B. S. Mechanistic Insights into the Selective Electroreduction of Carbon Dioxide to Ethylene on Cu2O-Derived Copper Catalysts. *J. Phys. Chem. C* **2016**, *120*, 20058−20067.
(35) Dutta, A.; Rahaman, M.; Luedi, N. C.; Mohos, M.; Broekmann, P. Morphology Matters: Tuning the Product Distribution of CO2 Electroreduction on Oxide-Derived Cu Foam Catalysts. *ACS Catal.* **2016**, *6*, 3804−3814.
(36) Lee, S.; Park, G.; Lee, J. Importance of Ag-Cu Biphasic Boundaries for Selective Electrochemical Reduction of CO2 to Ethanol. *ACS Catal.* **2017**, *7*, 8594−8604.

https://doi.org/10.1021/acsaem.3c00985
ACS Appl. Energy Mater. 2023, 6, 7571−7577